Direct Observation of Protein−Ligand Interaction Kinetics†

Tanja Mittag,‡ Brian Schaffhausen,§ and Ulrich L. Günther*,‡

Center for Biomolecular Magnetic Resonance, Biocentre N230, J. W. Goethe University, Frankfurt, Marie-Curie-Strasse 9, 60439 Frankfurt, Germany, and Department of Biochemistry, School of Medicine, Tufts University, 136 Harrison Avenue, Boston, Massachusetts 02111

Received May 8, 2003; Revised Manuscript Received July 9, 2003

ABSTRACT: Internal dynamics on the micro- to millisecond time scale have a strong influence on the affinity and specificity with which a protein binds ligands. This time scale is accessible through relaxation dispersion measurements using NMR. By studying the dynamics of a protein with different concentrations of a ligand, one can determine the dynamic effects induced by the ligand. Here we have studied slow internal dynamics of the N-terminal src homology 2 domain of phosphatidylinositide 3-kinase to probe the role of individual residues for the interaction with a tyrosine-phosphorylated binding sequence from polyoma middle T antigen. While slow dynamic motion was restricted to a few residues in the free SH2 and in the SH2 complex, motion was significantly enhanced by adding even small amounts of ligand. Kinetic rates induced by ligand binding varied between 300 and 2000 s^{-1}. High rates reflected direct interactions with the ligand or rearrangements caused by ligand binding. Large differences in rates were observed for residues adjacent in the primary sequence reflecting their individual roles in ligand interaction. However, rates were similar for residues involved in the same side chain interactions, reflecting concerted motions during ligand binding. For a subset of residues, exchange must involve structural intermediates which play a crucial role in high-affinity ligand binding. This analysis supports a new view of the dynamics of individual sites of a protein during ligand interaction.

Protein function strongly depends on changes in three-dimensional structure in response to specific molecular interactions (*1*). In enzymes, for example, access of the ligand to the catalytic site may require conformational rearrangements to provide a path of entry. Proteins that regulate signal transduction often undergo significant conformational changes in tertiary structure upon ligand binding (*2*). Protein interactions which involve rearrangements strongly depend on the internal dynamics of the protein. A detailed analysis of protein dynamics will thus provide valuable information for the understanding of protein−ligand interactions. NMR relaxation experiments have proven to be a powerful tool in extracting dynamic parameters at atomic resolution (*3*, *4*). In the past, most relaxation studies concentrated on fast picosecond to nanosecond dynamics. More recently, there has been increased interest in dynamics at a microsecond to millisecond time scale. The inherent dynamics on this time scale are biologically relevant because this is the time scale of many protein−ligand interactions (*5*). Such slow dynamic processes may involve concerted motions of larger parts of a protein which are relevant for biological function.

NMR spectroscopy provides several possibilities for measuring dynamics on slow time scales. The broadening and shape of protein signals for various ligand concentrations can be used to determine kinetic rates (*6*). Chemical exchange rates on a micro- to millisecond time scale can be obtained from relaxation dispersion using Carr−Purcell−Meiboom−Gill (CPMG)[1] sequences. CPMG measurements have previously been used to detect exchange between different conformational states of proteins and have been used to determine kinetic rates involving states with low populations (*7*, *8*). Recently, Eisenmesser *et al.* (*9*) used CPMG measurements to determine the catalytic turnover rates for individual residues in cyclophilin A by separating the catalytic rate from internal dynamics.

We have been using the N-terminal src homology 2 domain (SH2) of phosphatidylinositide 3-kinase (PI3K) that interacts with phosphotyrosine (ptyr) containing sequences from ligands such as the platelet-derived growth factor (PDGF) receptor or polyoma middle T antigen (MT) as a model to examine protein−ligand interactions using NMR. PI3 kinases are important for cell function (*10*−*18*). Interaction of PI3K with middle T ligand is critical for induction of tumors by polyomavirus (*19*). Intracellular trafficking of PI3K is mediated by the binding of the SH2s to tyrosine-phosphorylated sequences of oncogenes such as MT (*20*) or receptors such as PDGFr (*21*, *22*). The structure of N-SH2 is known from both NMR and X-ray studies (*23*−*26*). As for other SH2s, it can be described as a central antiparallel β-sheet flanked by smaller β-sheets and two α-helices. SH2s

† This work was supported by the Large Scale Facility Frankfurt (UNIFRANMR), by a stipend of the Deutsche Studienstiftung (T.M.), and by grants from the National Institutes of Health (B.S.).

* To whom correspondence should be addressed. Telephone: 49-(0)69-79829623. Fax: 49-(0)69-79829632. E-mail: Ulrich.Guenther@em.uni-frankfurt.de.

‡ J. W. Goethe University, Frankfurt.

§ Tufts University.

[1] Abbreviations: CPMG, Carr−Purcell−Meiboom−Gill; GST, glutathione *S*-transferase; HSQC, heteronuclear single-quantum coherence; MT, polyomavirus middle T antigen; MT8, EEEpYMPME-NH_2; N-SH2, N-terminal src homology 2 domain of p85; PDGFr, platelet-derived growth factor receptor; PI3K, phosphatidylinositide 3-kinase; ptyr, phosphotyrosine.

10.1021/bi0347499 CCC: $25.00
Published on Web 08/30/2003

bind tyrosine-phosphorylated sequences with specificity being largely determined by the three residues C-terminal to the tyrosine. Our NMR studies have suggested that the structure is interactive in the sense that changes at the ptyr +1 or +3 position C-terminal to the ptyr can have effects throughout the structure (*27*). Very recently, we have shown how line shape analysis can be used to demonstrate the existence of structural intermediates in the binding process and to measure local off-rates (*6* and unpublished data).

Here we use the ability of CPMG measurements to detect motion on the micro- to millisecond time scale to probe the behavior of N-SH2. Separation of internal dynamics and dynamics associated with ligand interaction was achieved by measuring relaxation dispersion for samples with different concentrations of the ligand. We used this information for a kinetic analysis of the interaction of SH2 with a phosphorylated high-affinity peptide derived from the binding site of MT.

MATERIALS AND METHODS

The peptide EEEpY$_{315}$MPME-NH$_2$ (MT8) was synthesized and HPLC purified by the Tufts Protein Chemistry Facility as described previously (*27*). The purity was confirmed by NMR spectra and ESI and MALDI mass spectra.

Protein samples were prepared as described previously (*27*, *29*) using 1 L of CELTONE-CN (MARTEK Biosciences Corp.). NMR sample conditions were 0.5 mM ^{15}N-labeled N-SH2 in 0.1 M KCl (pH 6.8) and a 90% H_2O/10% D_2O mixture in a sample volume of 450 μL.

All NMR spectra were recorded at 303 K. Relaxation dispersion data were obtained at two static magnetic fields, corresponding to proton Larmor frequencies of 500 and 700 MHz (in some cases 500 and 800 MHz) using a relaxation-compensated CPMG dispersion experiment performed in a constant time manner (*8*). Spectra were collected as a series of 14−16 two-dimensional (2D) spectra with CPMG field strengths (ν_{cp}) of 17, 33, 50, 67, 83, 100, 117, 133, 167, 200, 233, 267, 333, 400, 500, and 667 Hz. Repeated experiments were performed at 33 and 500 Hz. The constant time period was set to 60 ms; the reference experiment was carried out by omitting the CPMG period. Spectra were acquired with at least 1024 × 128 complex points. Processing and analysis of the NMR spectra were performed with the use of NMRlab (*30*).

Chemical exchange on a micro- to millisecond time scale increases the value of R_2 by an amount R_{ex}. The exchange contribution R_{ex} in the measured transverse relaxation time is minimal for fast refocusing rates in CPMG pulse trains. For varying echo times, relaxation dispersion curves are obtained which depend on the chemical shift differences ($\Delta\omega$), the population of the two states, and the exchange rate k_{ex}.

Exchange rates (k_{ex}) were determined by fitting relaxation dispersion curves to the general expression for the phenomenological transverse relaxation rate constant in the case of two-site exchange with $p_B = 1 - p_A$ (*31*−*34*):

$$R_2(1/\tau_{cp}) = {}^1/_2\left\{R_{2A}^0 + R_{2B}^0 + k_{ex} - \frac{1}{2\tau_{cp}}\cosh^{-1}[D_+\cosh(\eta_+) - D_-\cos(\eta_-)]\right\} \quad (1)$$

where $2\tau_{cp}$ is the delay between 180° pulses in the CPMG pulse train and

$$D_\pm = \frac{1}{2}\left[\pm 1 + \frac{\Psi + 2\Delta\omega^2}{(\Psi^2 + \zeta^2)^{1/2}}\right]$$

$$\eta_\pm = \sqrt{2}\tau_{cp}[\pm\Psi + (\Psi^2 + \zeta^2)^{1/2}]^{1/2}$$

$$\Psi = (R_{2A}^0 - R_{2B}^0 - p_A k_{ex} + p_B k_{ex})^2 - \Delta\omega^2 + 4p_A p_B k_{ex}{}^2$$

$$\zeta = 2\Delta\omega(R_{2A}^0 - R_{2B}^0 - p_A k_{ex} + p_B k_{ex})$$

The refocusing field is related to the delay $2\tau_{cp}$ between to 180° pulses according to $\nu_{cp} = 1/(4\tau_{cp})$.

Simulations of eq 1 with different relaxation rates R_{2A}^0 and R_{2B}^0 for the amide nitrogens of sites A and B show only a minor effect on the dispersion curves compared to simulations in which $R_{2A}^0 = R_{2B}^0 = R_2^0$. This effect is most pronounced for very fast refocusing rates ($\nu_{cp} \rightarrow \infty$). However, relaxation dispersion at very high refocusing rates has little influence on the values of k_{ex}, $\Delta\omega$, p_A, and p_B; it mainly correlates with R_2^0. Since the difference between transverse ^{15}N relaxation rates of the exchanging partners is not very high, we have assumed that R_{2A}^0 and R_{2B}^0 are equal. When the chemical shifts of the two states are known, $\Delta\omega$ can be fixed at the value of the chemical shift difference. The chemical shift time regime can be determined from the static magnetic field dependence of the exchange contribution to R_2. The parameter

$$\alpha = \left(\frac{B_{02} + B_{01}}{B_{02} - B_{01}}\right)\left(\frac{R_{ex2} - R_{ex1}}{R_{ex2} + R_{ex1}}\right) \quad (2)$$

where R_{ex1} and R_{ex2} are the exchange contributions to the transverse relaxation rate at static magnetic field strengths B_{01} and B_{02}, respectively, equals 1 for intermediate exchange. When $0 < \alpha < 1$, the exchange is slow on the NMR time scale, and when $1 < \alpha < 2$, it is fast. R_{ex} was obtained from the difference in the effective transverse relaxation rate in the absence and presence of a high refocusing field [$R_{ex} = R_2(\nu_{cp} \rightarrow 0) - R_2(\nu_{cp} \rightarrow \infty)$]. Since the time regime detected by relaxation dispersion is determined by the ratio of k_{ex} and $\Delta\omega$ which is determined in a manner independent of α, this parameter is useful in assessing the consistency of the data analysis.

For exchange between two sites

$$A \underset{k_{BA}}{\overset{k_{AB}}{\rightleftharpoons}} B$$

the measured exchange rate k_{ex} equals $k_{AB} + k_{BA}$. If the exchanging sites are the free and the complexed form of a protein

$$P + L \underset{k_{off}}{\overset{k_{on}}{\rightleftharpoons}} PL$$

the exchange rate k_{ex} equals $k_{on}[L] + k_{off}$. In the special case where the concentration of the ligand is low, the equilibrium concentration [L] will be minimal for high affinities. Therefore, the measured exchange rate approaches the off-

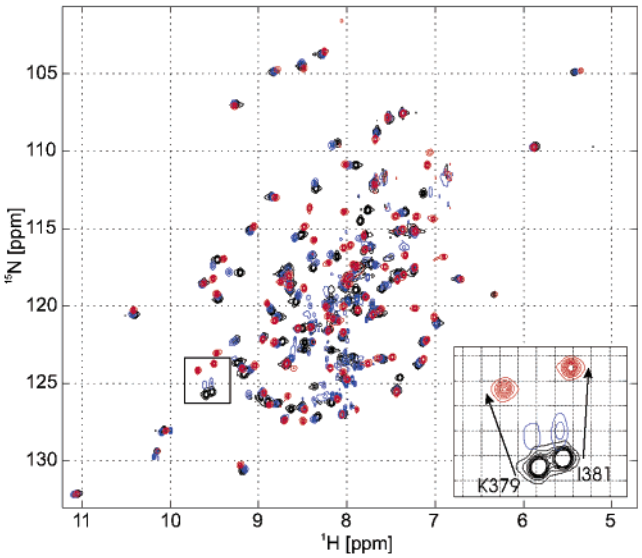

FIGURE 1: ^{1}H−^{15}N HSQC spectra of PI3K N-SH2 in the free state (black), an initial binding state with $^{1}/_{20}$ of the stoichiometric amount of the MT8 peptide (blue), and the SH2−MT8 complex (red). In the spectrum recorded for an initial binding state, the resonances are shifted only slightly while lines of K379 and I381 (expansion) are broadened.

rate ($k_{ex} \approx k_{off}$), and the free form is usually the only observable species ($p_P \gg p_{PL}$).

RESULTS

We have characterized motions in N-SH2 associated with the binding of an eight-amino acid peptide EEEpYMPME-NH_2 (MT8) derived from the SH2 binding region of MT antigen. ^{15}N relaxation dispersion was assessed by measuring transverse relaxation rate constants with varying delays between refocusing pulses (relaxation dispersion). This was done for the backbone amides of p85 N-SH2 in three different states: (1) free N-SH2, (2) a saturated N-SH2−MT8 complex, and (3) a partially titrated N-SH2 with only $^{1}/_{20}$ of the stoichiometric equivalent of peptide required for full titration. The corresponding ^{15}N HSQC spectra are shown in Figure 1. Relaxation dispersion curves were analyzed by fitting the data to eq 1 by optimizing k_{ex}, $\Delta\omega$, and the populations of the states. Results of these simulations are presented in Tables 1−4. Differences in relaxation parameters between the three states were used to examine the dynamics of the binding process and to derive the kinetic rates of the interaction.

Exchange in Free SH2. We have analyzed relaxation dispersion for 94 residues for which the resonances were not overlapped in the HSQC spectrum which is shown in black in Figure 1. Examples of typical dispersion curves are shown in panels a and b of Figure 2 for residues D337 and I338. For most residues, the transverse relaxation rate R_2 was not influenced by the refocusing rate, ν_{cp}, of the CPMG sequence. This means there was no contribution from R_{ex} to the transverse relaxation rate R_2. Most residues in the α-helices and in the β-sheet did not undergo exchange processes. However, we observed small exchange contributions R_{ex} for 15 residues listed in Table 1. The exchanging residues are also depicted in Figure 3a on a ribbon diagram of p85 N-SH2 which is labeled with colors from blue to red for increasing values of R_{ex}.

Table 1: ^{15}N Relaxation Dispersion Parameters of Exchanging Residues of Free SH2

residue	R_{ex} (s^{-1})[a]	$\Delta\omega_{eval}$ (ppm)	k_{ex} (s^{-1})	p_a	$R_2^0(\nu_{cp} \rightarrow \infty)$ (s^{-1})	α
Y368	2.3	1.94	894	0.99	15.42	1.24
R373	2.2	0.28	1687	0.5	14.62	1.95
K374	2.0	0.94	91	0.98	18.42	0.18
I383[b]	5.2	1.77	620	0.99	14.14	0.92
F384[b]	13.8	0.20	16	0.5	13.76	1.70
Y390	3.8	0.88	815	0.91	13.68	1.72
G391[b]	2.4	0.73	572	0.98	12.53	1.58
F392[b]	4.2	1.04	442	0.98	13.81	1.13
S393	2.8	3.16	549	0.99	10.60	0.39
L396[b]	2.3	4.34	5	0.5	13.17	0.05
T397	2.8	0.19	590	0.5	17.35	1.95
F398	2.8	3.34	6	0.5	12.82	0.03
N399	2.0	0.69	118	0.98	16.02	0.48
N410[b]	6.0	0.65	487	0.96	21.02	1.59
S412[b]	1.7	1.56	287	0.99	12.91	0.41

[a] $R_{ex} = R_2(\nu_{cp} \rightarrow 0) - R_2(\nu_{cp} \rightarrow \infty)$. [b] Data from 500 and 800 MHz were analyzed.

Table 2: Effective Transverse Relaxation Rates at High and Low Refocusing Field Strengths for Residues with Low Signal-to-Noise Ratios

residue	$R_2(\nu_{cp} = 667$ Hz) (s^{-1})	$R_2(\nu_{cp} = 17$ Hz) (s^{-1})
free SH2		
R340	26.2	27.0
G366	28.2	32.6
D394	20.5	25.0
R409	25.0	24.8
N417	38.6	48.5
V422	17.4	21.8
L424	28.3	31.3
intermediate state		
R409	19.2	23.5
A414	16.3	22.8
V422	21.8	26.1
SH2−MT8 complex		
D394	25.1	28.2
A414	14.8	26.0

The exchange contribution R_{ex} to the total transverse relaxation rate R_2 is a qualitative measure of exchange processes on a micro- to millisecond time scale. Enhanced values of R_{ex} were observed for some residues in the central β-sheet close to the EF loop (I383 in βD and F384 in βD′) and for N410 in the BG loop. Interestingly, none of the residues in the ptyr binding pocket exhibited exchange, except R340, one of the arginines involved in the coordination of the ptyr phosphate. For R340 in the ptyr binding pocket, for residues R409, N417, V422, and L424 in the BG loop, and for D394 in the EF loop and one residue in the BC loop (G366), high values of R_2 even at high refocusing rates (Table 2) indicated exchange at a relatively high rate ($k_{ex} > 2000$ s^{-1}). These residues are labeled orange in Figure 3a. Although the exchange contribution must be high in the BG loop, quantitative values for exchange parameters R_{ex} and k_{ex} could not be derived because of the high R_2 and the resulting low signal intensity. High mobility is probably also the reason why resonances of residues S361−H365 from the BC loop cannot be observed in any of our spectra, even at high refocusing rates in CPMG experiments. This view is supported by the exchange contribution observed at the edge of the BC loop for G366.

Table 3: ^{15}N Relaxation Dispersion Parameters of Exchanging Residues of SH2 in the Initial Binding State

residue	R_{ex} (s^{-1})[a]	$\Delta\omega_{titr}$ (ppm)[b]	$\Delta\omega_{eval}$ (ppm)[c]	k_{ex} (s^{-1})	p_a	R_2^0 (s^{-1})	α
D330	4.3	0.04	2.95	843	0.99	13.88	0.78
S339	16.4	0.75		1478	0.65	16.00	1.95
R340	4.6	0.55		1345	0.87	17.11	1.93
E341	1.9	0.22		1252	0.50	12.92	1.95
N344	7.9	0.51		1536	0.50	13.28	1.95
E345[d]	6.5	0.56		1033	0.87	12.50	−
V357[e]	3.0	0.28		660	0.50	15.20	−
R358	7	0.51		1252	0.50	16.56	1.96
D367[e]	4.1	1.31		917	0.97	12.51	−
Y368	17.8	0.32	5.28	1937	0.98	12.75	1.01
T369	28.8	1.21	2.64	766	0.95	19.21	0.79
N378	4.5	0.31		981	0.50	13.42	1.95
K379[e]	57	1.75		1157	0.67	19.50	−
S380	2.4	0.30	2.15	87	0.97	15.4	0.04
I381[e]	56	1.48		636	0.74	26.98	−
I383[e]	25.8	1.81		1706	0.83	16.74	−
F384	4.9	0.44		521	0.91	14.68	1.85
H385	4.1	0.20	2.33	460	0.99	14.18	0.48
R386[f]	4.9	0.13	1.33	813	0.98	12.78	1.41
Y390	3.5	0.41		1203	0.84	14.28	1.94
G391	3.3	0.16		315	0.50	14.46	1.96
F392	15.9	0.92		1745	0.77	14.78	1.94
S393	6.6	0.39	3.05	518	0.99	12.08	0.37
L396	4.4	0.09	4.67	634	0.99	13.43	0.25
E403	2.8	0.19		355	0.80	15.14	1.93
L404	2.9	0.24		913	0.50	14.48	1.95
N406	8.9	0.65		1806	0.72	12.92	1.95
N410[e]	40	1.71		1791	0.50	18.70	−
S412	27.9	1.30		2118	0.75	13.08	1.94

[a] $R_{ex} = R_2(\nu_{cp} \rightarrow 0) - R_2(\nu_{cp} \rightarrow \infty)$. [b] Chemical shift difference of the amide nitrogen between free N-SH2 and the N-SH2−MT8 complex. [c] Fitted value for $\Delta\omega$, not given when $\Delta\omega_{titr}$ was used to fit the data. [d] Data from only 700 MHz were used. [e] Data from only 500 MHz were used. [f] Data from 500 and 800 MHz were analyzed.

Table 4: ^{15}N Relaxation Dispersion Parameters of Exchanging Residues of the SH2−MT8 Complex

residue	R_{ex} (s^{-1})[a]	$\Delta\omega_{titr}$ (ppm)[b]	$\Delta\omega_{eval}$ (ppm)[c]	k_{ex} (s^{-1})	p_a	$R_2^0(\nu_{cp} \rightarrow \infty)$ (s^{-1})	α
R340[d]	4.2	0.55		399	0.92	25.65	−
E342	1.2	0.03	0.39	46	0.97	12.09	0.46
A351	5.8	0.07	1.46	782	0.98	17.00	1.39
Y368[d]	2.0	0.32		558	0.85	19.33	−
R373[d]	3.4	0.17	0.84	297	0.98	18.18	−
K374	1.7	0.26		349	0.94	13.18	1.86
K379	3.7	1.75		1026	0.99	13.00	1.44
S380	2.7	0.30		27	0.89	14.60	0.91
I381	4.4	1.48		648	0.99	14.45	1.20
R386	1.6	0.13	1.83	38	0.96	13.18	0.02
Y390	3.5	0.41		832	0.89	13.53	1.91
S393	2.5	0.39		537	0.94	12.22	1.86
L396	3.0	0.09	1.69	674	0.99	15.69	1.11
V401	3.7	0.25		727	0.58	16.49	1.95
N410	4.3	1.71		967	0.98	16.64	−
S412	3.8	1.30		1323	0.98	14.75	1.75
Y416	20.9	3.40		1518	0.96	19.76	−
L420	4.6	1.91		1329	0.99	13.41	1.56

[a] $R_{ex} = R_2(\nu_{cp} \rightarrow 0) - R_2(\nu_{cp} \rightarrow \infty)$. [b] Chemical shift difference of the amide nitrogen between free N-SH2 and the N-SH2−MT8 complex. [c] Fitted value for $\Delta\omega$, not given when $\Delta\omega_{titr}$ was used to fit the data. [d] Data from only 500 MHz were used.

Exchange in the Initial Binding Step. The successive addition of peptide to N-SH2 causes progressively shifting resonances for 51 of 108 residues (*6*). Observation of a single set of shifting resonances with a chemical shift reflecting the populations of both states indicates fast exchange on the NMR time scale ($k_{ex} \gg \Delta\omega$). This was observed for most residues, although more complicated line shapes with signal shoulders in intermediate titration steps were observed for a subset of residues. These were previously interpreted to represent intermediate conformational states (*6*). To study the dynamics induced by peptide binding, we added a low concentration ($^1/_{20}$ of the stoichiometric equivalent of protein) of the EEEpYMPME-NH_2 peptide (MT8 peptide). The HSQC spectrum of this state is shown in blue in Figure 1. Relaxation rates for many residues of this sample represent a steady state view of the relaxation of the protein from a ligand-bound form to the state of the free protein. Since the exchange partners may also be different conformers of the protein, we have analyzed relaxation dispersion for all 94 residues for which the resonances were not overlapped in the HSQC spectrum. This included many residues for which no ^{15}N chemical shift perturbation was observed in ligand binding for detection of possible intermediates not seen in the titration.

For this low concentration of ligand, the resonances were shifted only slightly from their position in free SH2. It also is important to note that none of the resonances exhibited slowly exchanging signal components. The lines of many residues were broadened as a consequence of exchange initiated by the presence of the ligand (e.g., for residues K379 and I381 which are known to be involved in the binding process and whose amide resonances are depicted in the expansion in Figure 1). For many residues, the exchange contribution R_{ex} was significantly enhanced compared to those of the free and complexed states. This is depicted in Figure 3b where residues which exhibit enhanced exchange are grouped around the ptyr binding pocket (S339, R340, E341, V357, and R358), in regions of the central β-sheet which interact with the peptide (N378, K379, S380, I381, I383, F384, H385, and R386), in the EF loop (Y390, G391, F392, S393, and L396), and in the BG loop (R409, N410, S412, and A414). Enhanced exchange for S393 compared to the free SH2 is depicted in panels c and d of Figure 2, which shows the relaxation dispersion curves of S393 in the different states of the protein. The highest exchange contributions were observed in βD for residues K379, I381, and I383, at the tip of the EF loop for F392, and in the BG loop for N410 and S412 (Table 3). For some residues in the BG loop (413−422), high values of R_2 caused intensities that were too low to fit relaxation dispersion curves. However, signal intensities for fast and slow refocusing rates were significantly different, indicating that the low signal intensity was a consequence of a high exchange contribution. This allowed at least a qualitative measure of exchange. Examples for this behavior include R409, A414, and V422 which are labeled orange in the ribbon diagram in Figure 3b. Relaxation rates in the limits of fast and slow pulsing are listed in Table 2. For residues Y408, Q415, Y416, and K419 in BG (labeled in yellow in Figure 3b), no signal was observed after addition of peptide which is another indication of very large amplitude exchange processes, although a quantitative value could not be obtained.

Exchange in the SH2−MT8 Complex. N-SH2 in a stoichiometric complex with MT8 is relatively rigid on a millisecond to microsecond time scale. The exchange process of R340 already observed in free SH2 is preserved, and an

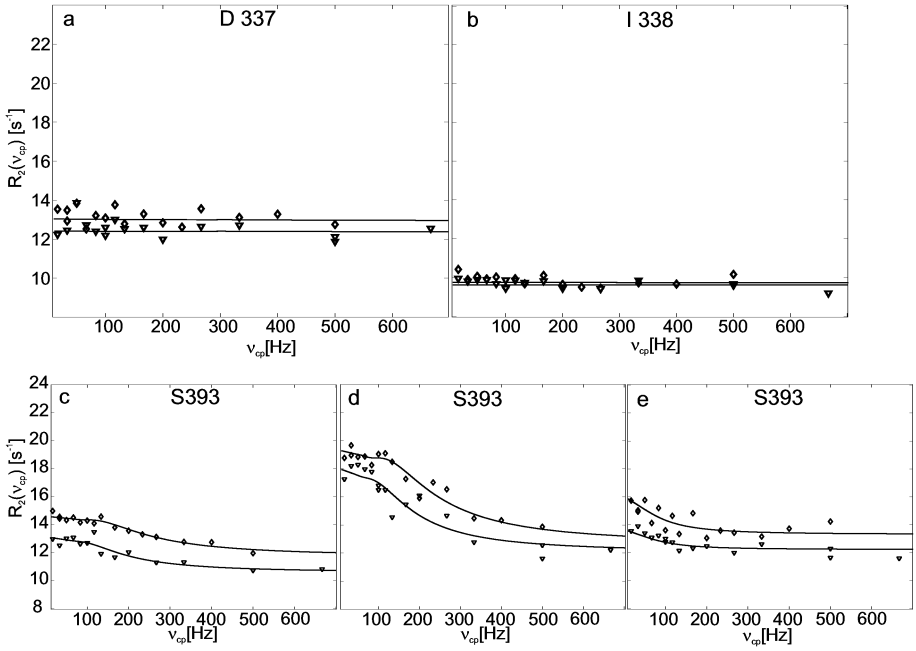

FIGURE 2: Effective transverse relaxation rates, R_2, as a function of the CPMG field strength, ν_{cp}. The values of R_2 for (a) D337 and (b) I338 of free SH2 do not depend on the field strength (no exchange on a millisecond time scale). Solid lines are straight lines with a value equal to the mean value of R_2. (c and d) Effective transverse relaxation rates, R_2, as a function of the CPMG field strength, ν_{cp}, for S393 (c) in free SH2, (d) in the initial binding state, and (e) in the SH2−MT8 complex. The best-fit dispersion curves using eq 1 are shown as solid lines. Data recorded at ^{1}H Larmor frequencies of 700 and 500 MHz are depicted with diamonds and triangles, respectively.

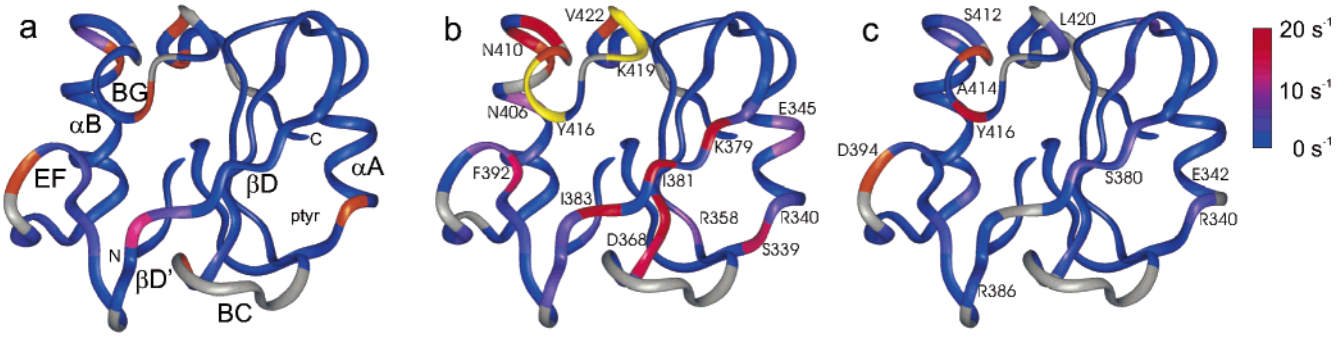

FIGURE 3: Exchange contributions for three different states of N-SH2. The exchange contribution R_{ex} to the ^{15}N transverse relaxation rate is depicted by color coding on the ribbon diagram of the SH2. The continuous color scale from blue to magenta to red (from 0 s^{-1} to 10 s^{-1} to 20 s^{-1}) represents the amplitude of R_{ex} for (a) free SH2, (b) SH2 in the initial binding state, and (c) the SH2−MT8 complex. Residues colored orange exhibit high exchange contributions which could not be quantified. Signals of residues colored yellow disappeared upon addition of ligand. Residues colored gray could not be analyzed due to overlap or missing assignments. The annotation of secondary structural elements follows the convention of Eck *et al.* (*35*).

additional residue in the ptyr binding pocket, E342, shows exchange (Figure 3c). The final complex behaved in a very different manner from that of the intermediate state. For example, residues in the β-sheet, the EF loop, and the BG loop exhibited very low amplitude exchange compared to the intermediate state.

Strikingly, some residues in the complex exhibited exchange contributions, although ligand binding did not cause any ^{15}N chemical shift change. This behavior was observed for residues E342, A351, R373, R386, and L396 which are labeled red in Figure 4b. Since exchange contributions to R_2 require a chemical shift change $\Delta\omega$, there must be some intermediate with a ^{15}N chemical shift different from that of free SH2. In this case, CPMG measurements can be used to detect exchanging conformers with low populations that cannot be detected in line shapes.

Exchange Rates. As shown in eq 1, relaxation dispersion depends on three important parameters: the population of exchanging sites, the chemical shift differences between exchanging partners, and the exchange rate k_{ex}. In the previous paragraph, the exchange contribution R_{ex} to R_2 has been described. While R_{ex} provides a qualitative measure of the amount of micro- to millisecond flexibility, k_{ex}, which describes the exchange rate, could be obtained for most exchanging residues. As mentioned earlier, for two-site exchange k_{ex} is defined as $k_{AB} + k_{BA}$, where k_{AB} is the forward reaction rate and k_{BA} is the backward reaction rate.

k_{ex} in Free N-SH2. Exchange rates are mapped on the ribbon diagram of SH2 in Figure 5a using a color scale from blue (0 Hz) to magenta (1000 Hz) to red (2000 Hz). The residues for which exchange rates were calculated are identical to those which exhibited exchange contributions R_e. Exchange rates were low in most parts of free SH2. Most residues in the β-sheet, the EF loop, and the BG loop exhibit exchange rates of ~400−600 s^{-1} (Table 1). Particularly low exchange rates were observed for K374 in upper βC (91 s^{-1}),

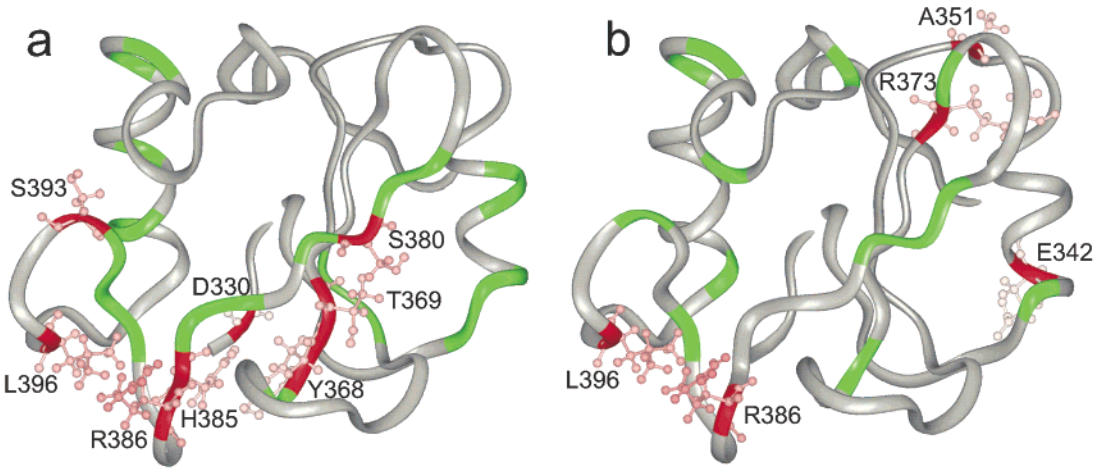

FIGURE 4: Conformational exchange (a) in SH2 in the initial binding state and (b) in the SH2−MT8 complex. The exchange contributions of residues colored green arise from binding and release of the ligand. The exchanging partners are the free and the complexed form of SH2. Their chemical shift difference was assumed in the relaxation dispersion analysis. For residues colored red, the chemical shift difference between the free protein and the complex could not explain the relaxation dispersion curves. Therefore, a different exchange partner must be assumed.

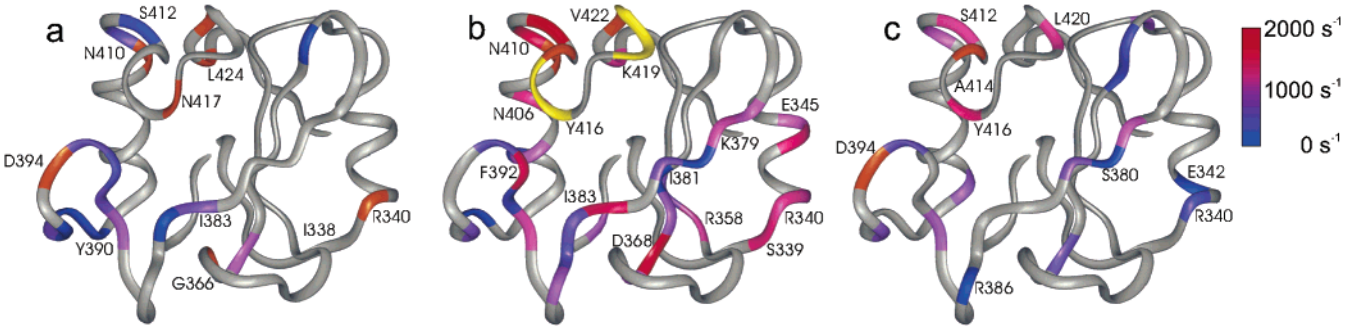

FIGURE 5: Exchange rates in three different states of N-SH2. The exchange rates k_{ex} are depicted by color coding on the ribbon diagram of SH2. A continuous color scale from blue to magenta to red (from 0 s^{-1} to 500 s^{-1} to 1000 s^{-1}) depicts k_{ex} for (a) free SH2, (b) SH2 in the initial binding state, and (c) the SH2−MT8 complex. Residues colored orange exhibit high exchange contributions which could not be quantified. Signals of residues colored yellow disappeared upon addition of ligand. Residues colored gray do not exhibit exchange or could not be analyzed due to overlap or missing assignments.

F384 in βD′ (16 s^{-1}), and L396 (5 s^{-1}) and F398 (6 s^{-1}) in the EF loop. Y368 in βC next to the BC loop and Y390 in the EF loop exhibited relatively high exchange rates of 894 and 815 s^{-1}, respectively.

k_{ex} in the Initial Binding Step. For exchange of one ligand molecule, k_{ex} also depends on the equilibrium concentration of free ligand $[L]_{eq}$ according to the equation $k_{ex} = k_{on}[L]_{eq} + k_{off}$, where k_{off} is the off-rate and k_{on} is the on-rate. For low concentrations of peptide and high affinities, the calculated exchange rates represent almost pure off-rates; i.e., $k_{ex} \approx k_{off}$. In the case of SH2 and the MT8 ligand, the affinity for the ligand was previously determined in competition binding of MT8 with ^{31}P-labeled MT antigen which gave an IC_{50} value of 8.4 μM (*27*). For an approximate dissociation constant K_D ($=k_{off}/k_{on}$) of 8 μM, a protein concentration of 0.5 mM, and addition of $^1/_{20}$ of the stoichiometric amount of peptide, the concentration of free ligand amounts to 4.3 $\times$ 10^{-7} M, and the occupancy of N-SH2 by MT8 is 4.9%. Only 1.7% of MT8 is not bound to protein.

For exchange induced by the addition of ligand, it is likely that the two exchanging partners are the free and the complexed states of the protein. Therefore, $\Delta\omega$ was set to the values of the ^{15}N chemical shift change of ligand binding if not otherwise indicated (Tables 3 and 4).

Exchange rates k_{ex} for the intermediate state of SH2 were significantly higher than those in free SH2 (Figure 5b). Nineteen residues exhibit exchange rates of 800−2000 s^{-1}, whereas exchange rates of 450−800 s^{-1} were obtained for only six residues. Particularly low exchange rates k_{ex} were obtained for S380 in βD (87 s^{-1}), G391 in the EF loop (315 s^{-1}), and E403 in αB (355 s^{-1}). Y368 next to the BC loop (1937 s^{-1}), I383 in βD (1706 s^{-1}), F392 in the EF loop (1745 s^{-1}), N406 and N410 in αB (1806 and 1791 s^{-1}, respectively), and S412 in the BG loop (2118 s^{-1}) exhibited particularly high exchange rates.

Interestingly, off-rates were often different for adjacent residues. For example, a sequence of residues in βD shows alternating rates. A low value of k_{ex} (87 s^{-1}) was observed for S380, and F382 does not exhibit exchange at all; on the other hand, the exchange rates of K379 (1157 s^{-1}), I381 (636 s^{-1}), and I383 (1706 s^{-1}) were significantly higher. K379, I381, and I383 point in the direction of the αB helix and the BG loop and are directly reflecting the binding reaction, whereas S380 is pointing toward the ptyr binding pocket. The off-rates of residues in the ptyr binding pocket were relatively homogeneous. The two conserved arginine residues coordinating the phosphotyrosine phosphate, R340 and R358, exhibited similar off-rates of 1345 and 1252 s^{-1}, respectively.

Similar off-rates were also observed for adjacent residues S339 and E341 (1478 and 1252 s^{-1}, respectively).

A subset of residues in and adjacent to loop regions (S393 in the EF loop, Y368 and T369 next to the BC loop, and H385, R386, and L396 next to the EF loop labeled in red in Figure 4a) exhibited relaxation dispersions which could not be interpreted adequately using the chemical shift difference between the free and complexed SH2 $\Delta\omega_{P-PL}$. The values of $\Delta\omega$ obtained by optimization of eq 1 are listed in Table 3. Thus, the exchanging partners are not the free, and the complexed protein and the exchange does not arise from binding and release of the ligand. In these cases, the exchange partners for free SH2 are most likely conformers formed upon ligand binding which act as intermediates on the reaction pathway. For all of these residues, the population of the minor state obtained from the simulation was $\leq 5\%$. The value of α was ≤ 1 except for that of R386, indicating exchange in the slow or intermediate time regime.

For those residues where the relaxation dispersion reflects the relaxation of the protein from the complexed to the free state, the parameter α (eq 2) approaches a value of 2, indicating fast exchange on the NMR time scale.

For most residues, the population of the predominant state obtained by fitting eq 1 to the relaxation dispersion data was between 0.8 and 0.99 (Table 3). These values are in concordance with a simple two-state binding reaction and reflect the expected mole fractions. However, for residues S339, E341, V357, and R358 in the ptyr binding pocket, N344 in the αA helix, N378 and K379 in βD, G391 in the EF loop, and L404 and N410 in the αB helix, we obtained populations of the minor state near 50% as obtained by optimization of eq 1. Assuming a one-step binding mechanism where the protein can only appear in a complexed state, the population of the minor state should not exceed 5%. Therefore, significantly enhanced populations of the minor state suggest the existence of protein intermediates stable on this time scale.

k_{ex} in the SH2−MT8 Complex. In the SH2−MT8 complex, the exchange contributions and exchange rates were both generally low compared to those for the sample with a small amount of ligand as depicted in Figure 5c. Exchange rates were in a similar range as those for free SH2. Exceptions were observed for E342 (46 s^{-1}), S380 (27 s^{-1}), and R386 (38 s^{-1}) with low exchange rates, whereas S412, Y416, and L420 in the BG loop exhibit particularly high exchange rates (1323, 1518, and 1329 s^{-1}, respectively).

DISCUSSION

Here we have compared the dynamics of free PI3K N-SH2 to those of the SH2−MT8 ligand complex. Internal motions in SH2 itself could be separated from dynamics induced by the interaction with the ligand by measuring relaxation dispersion in the free protein, the complexed protein, and an intermediate state with a low ligand concentration. This analysis supported the role of some key residues in the EF and BG loop together with residues in the central β-sheet which play a key role in ligand binding. Because we have previously used line shape analysis to examine the same ligand SH2 interaction, this work provides an opportunity to compare the value of the two approaches.

Relaxation dispersion measurements provide a detailed picture of the dynamics induced by SH2−ligand interaction. Dynamics in the free SH2 are minimal and mainly limited to the loop regions. The highest values of R_{ex} in BG are almost one order of magnitude smaller than those observed with ligand present. However, some residues in BG (orange in Figure 3a) showed low signal intensities with relatively high levels of exchange. These residues (R409, V422, and L424) may have a hinge function for the loop. Missing signals of residues in the BC loop are probably also a consequence of exchange. G366 at the edge of the BC loop exhibited high relaxation rates. Interestingly, the exchange contribution of F384 in βD had the highest value of R_{ex} with a very low exchange frequency. This may reflect the interaction of the F384 side chain with the BC loop. In previous line shape analyses, this residue exhibited conformational averaging when a ligand was present (*6*). The current analysis suggests that this residue already has a high flexibility on a slow time scale in free SH2.

To measure the dynamics of the interaction of the protein with the ligand, we added a small amount of ligand. Under steady state conditions, it is easily possible to separate the on-rate from the off-rate because the equilibrium concentration of the free ligand is minimal and therefore $k_{on}[L]_{eq}$ becomes negligible. The choice of a low concentration also had the advantage that signal intensities were still sufficiently large to observe signals in CPMG measurements at small refocusing rates. The chemical shift difference between the free and the fully complexed protein should represent the relevant chemical shift difference for the relaxation dispersion effect. Residues for which a good fit could be achieved using $\Delta\omega_{P-PL}$ are labeled green in Figure 4a. However, for a subset of residues, the chemical shift perturbation of ligand binding was too small to fit the relaxation dispersion curves. These residues are labeled red in Figure 4a. Fitting $\Delta\omega$ for these residues yielded small populations for another exchange partner, indicative of an unidentified intermediate on the reaction pathway. These residues are located in loop regions (S393 in the EF loop) and directly adjacent to loop regions (Y368 and T369 next to the BC loop and H385, R386, and L396 next to the EF loop). This supports our previous conclusion from line shape analysis that ligand binding requires the formation of intermediates for some residues (*6*). Some (D330, Y368, S380, H385, R386, and L396) of these residues for which relaxation measurements suggested intermediates exhibited hardly any chemical shift perturbation. In these instances, intermediates were detected that could not be observed by line shape analysis. For T396 and R386, some exchange was still observed in the complex. Consequently, exchange for these residues must be attributed to some conformational exchange and cannot be attributed to the dynamics of ligand binding. α values between 0 and 1 show that the conformational exchange of these residues is on the slow or intermediate NMR time regime. Signal shoulders in titration spectra further support the existence of slow motions.

The sudden increase in the level of exchange after addition of a small amount of ligand gives an impressive picture of the dynamics in the protein resulting from the ligand interaction. Because there was comparably slow exchange in free SH2 and in the SH2 complex, the high level of exchange observed in the intermediate binding state can be attributed to the relaxation of the protein complex back to free SH2. This is not necessarily the off-rate of the ligand

because the lifetime of the bound state of the protein may be longer than the lifetime of the interaction with the ligand. This may be particularly important if the relaxation to the free state requires complex concerted rearrangements in the protein.

The overall picture of exchange contribution with a small amount of ligand shown in Figure 1b indicates the rearrangements induced by ligand binding and direct ligand interaction. Interestingly, R_{ex} alternates between very high and low values in a sequence of residues from K379 to F384 in βD. Those residues which point toward the BG and EF loops (K379, I381, and I383) adopt high values representing the dynamics of the interaction with the peptide. In contrast, S380 and F384 exhibit lower values and K382 exhibits no exchange. This result suggests that motions observed on the amide ^{15}N reflect motions of side chains which may be correlated through space. For example, the rates of I383 and F384 correlate well with rates in the EF loop and that of K379 correlates with rates in the BG loop, suggesting concerted motion of those residues.

The rearrangement of the BG loop is reflected in high values in the hinge region (N410, S412, A414−Y416, K419, and V422) on each side of the loop. Some residues in the BG loop can no longer be analyzed because of the high dynamics in this loop. Interestingly, F392 at the tip of the EF loop has the greatest exchange contribution in this loop. As previously reported, the EF loop and the BG loop are linked by a stacking interaction of the aromatic side chains of F392 and Y416 in the free protein (*26*). Upon ligand binding, this interaction is dissolved which is reflected in high exchange contributions for both residues.

Very high exchange contributions were also observed for residues Y368 and T369 in βC, at the edge of the BC loop, which support the role of the BC loop region for the interaction with the ligand (*25*). Rearrangements in this region of the protein seem to be important for reshaping the ptyr binding pocket for effective high-affinity interaction.

In the ptyr binding pocket, rates of adjacent residues are similar and reflect the off-rate of the ligand in this region. Similar rates are observed for residues S339 and R340, one of the two arginines which coordinate the ptyr phosphate, and E341. Interestingly, the measured rate is similar for R358, the arginine which coordinates the ptyr phosphate from the other side.

In the final complex, Y416 is the only residue which exhibits a large exchange contribution. Y416 had been identified as a residue which undergoes a large movement upon ligand binding (*25*, *26*) and exhibited a large chemical shift perturbation of 3.4 ppm (*27*). Interestingly, exchange for this and some adjacent residues (N410, S412, and L420) was not completely frozen in the complex. The large chemical shift change upon ligand binding is responsible for the high relaxation dispersion effect.

The off-rates determined here can be compared to off-rates previously determined using line shape analysis (*6*). Off-rates of S339 [1478 s^{-1} from dispersion analysis vs 1120 (−220 to +310) s^{-1} from line shape analysis], R340 (1345 vs 1500 s^{-1}), K379 [1157 vs 930 (−100 to +120) s^{-1}], and H385 [460 vs 560 (−80 to +110) s^{-1}] obtained from relaxation dispersion analysis and line shape analysis were similar within experimental error. For some residues, however, the results from relaxation dispersion and line shape analysis did not agree. Line shape analysis yielded values for k_{off} of 550 s^{-1} for F392 and 600 s^{-1} for S412. From relaxation dispersion, we obtained much higher rates, 1745 s^{-1} for F392 and 2118 s^{-1} for S412. These differences may be a consequence of the systematic error made by the assumption of two-state exchange used in the analysis. If the actual mechanism of the interaction involves more than two states, intermediates must be taken into account for the analysis. How does this affect the rates obtained from line shapes and relaxation dispersion? Clearly, intermediates which are not observed will reduce the intensity of the signals for intermediate ligand concentrations. There line shape analysis will yield a rate which is too low. However, relaxation dispersion will show an increased R_2 starting at the highest rate that is involved in a set of parallel processes. In these cases, the rates measured by the CPMG method will always be higher than the rates obtained from line shapes. Interestingly, some of the residues that exhibited very high exchange contributions in the intermediate state exhibited complex lines. K379 and F392 exhibit minor shoulders in one or two lines of the titration, whereas S412 exhibited significantly distorted lines during the titration with disappearing signals. The existence of intermediate states may also be supported by relaxation dispersion curves which could not be fitted using the $\Delta\omega$ from the ligand binding. In these cases, some other conformer must be responsible for the exchange effect. Such conformers may represent intermediates in ligand binding.

There are clearly differences between CPMG and line shape analysis for the examination of molecular dynamics. CPMG is not applied to residues that shift only in the proton dimension (e.g., A360 in the beginning of the BC loop). Line shape analysis clearly emphasizes the complexity of the binding mechanism, while relaxation dispersion gives only rudimentary information about intermediates in ligand binding. However, unlike line shape analysis, CPMG analysis can detect intermediates even if there is no chemical shift difference between free SH2 and the final complex (e.g., D330). Relaxation dispersion analysis also shows conformational exchange in the free protein and in the final complex which cannot be analyzed in line shape analysis.

The overall conclusions from relaxation dispersion and line shape analysis are similar. Both methods provide a direct view of the kinetic events caused by ligand binding at the site of individual amino acids. This analysis supports the role of key regions of the protein such as the ptyr binding pocket and the central β-sheet. An important role of the BG loop and the EF loop is indicated in both analyses. Most importantly, there must be structural intermediates on the binding pathway. In fact, extensive conformational exchange was induced by small amounts of ligand. The nature and location of conformational exchange are important for high-affinity ligand binding. This is a new aspect in the description of protein−ligand interactions which has important theoretical and practical consequences.

ACKNOWLEDGMENT

We thank H. Rüterjans for kindly giving U.L.G. access to his laboratory.

REFERENCES

1. Karplus, M., and McCammon, J. A. (1983) Dynamics of proteins: elements and function, *Annu. Rev. Biochem. 53*, 263−300.

2. Pawson, T. (1995) Protein modules and signalling networks, *Nature 373*, 573−580.
3. Palmer, A. G. (1997) Probing molecular motion by NMR, *Curr. Opin. Struct. Biol. 7*, 732−737.
4. Kay, L. E. (1998) Protein dynamics from NMR, *Nat. Struct. Biol. NMR Suppl. 5*, 513−517.
5. Fersht, A. (1999) *Structure and Mechanism in Protein Science. A Guide to Enzyme Catalysis and Protein Folding*, 1st ed., Freeman, New York.
6. Günther, U., Mittag, T., and Schaffhausen, B. (2002) Probing src homology 2 domain ligand interactions by differential line broadening, *Biochemistry 41*, 11658−11669.
7. Palmer, A. G., Kroenke, C. D., and Loria, J. P. (2001) Nuclear magnetic resonance methods for quantifying microsecond-to-millisecond motions in biological macromolecules, *Methods Enzymol. 339*, 204.
8. Tollinger, M., Skrynnikov, N. R., Mulder, F. A. A., Forman-Kay, J. D., and Kay, L. E. (2001) Slow dynamics in folded and unfolded states of an SH3 domain, *J. Am. Chem. Soc. 123*, 11341−11352.
9. Eisenmesser, E. Z., Bosco, D. A., Akke, M., and Kern, D. (2002) Enzyme dynamics during catalysis, *Science 295*, 1520−1523.
10. Vanhaesebroeck, B., and Waterfield, M. (1999) Signaling by distinct classes of phosphoinositide 3-kinases, *Exp. Cell Res. 253*, 239−254.
11. Dankort, D., and Muller, W. (2000) Signal transduction in mammary tumorigenesis: a transgenic perspective, *Oncogene 19*, 1038−1044.
12. Datta, S., Brunet, A., and Greenberg, M. (1999) Cellular survival: a play in three Akts, *Genes Dev. 13*, 2905−2927.
13. Wurmser, A., Gary, J., and Emr, S. (1999) Phosphoinositide 3-kinases and their FYVE domain-containing effectors as regulators of vacuolar/lysosomal membrane trafficking pathways, *J. Biol. Chem. 274*, 9129−9132.
14. Rameh, L., and Cantley, L. (1999) The role of phosphoinositide 3-kinase lipid products in cell function, *J. Biol. Chem. 274*, 8347−8350.
15. Corvera, S., D'Arrigo, A., and Stenmark, H. (1999) Phosphoinositides in membrane traffic, *Curr. Opin. Cell Biol. 11*, 460−465.
16. Wymann, M., and Pirola, L. (1998) Structure and function of phosphoinositide 3-kinases, *Biochim. Biophys. Acta 1436*, 127−150.
17. Krugmann, S., and Welch, H. (1998) PI 3-kinase, *Curr. Biol. 8*, R828.
18. Fruman, D., Meyers, R., and Cantley, L. (1998) Phosphoinositide kinases, *Annu. Rev. Biochem. 67*, 481−507.
19. Freund, R., Dawe, C. J., Carrol, J. P., and Benjamin, T. L. (1992) Changes in frequency, morphology, and behavior of tumors induced in mice by a polyoma virus mutant with a specifically altered oncogene, *Am. J. Pathol. 141*, 1409−1425.
20. Yoakim, M., Hou, W., Liu, Y., Carpenter, C. L., Kapeller, R., and Schaffhausen, B. S. (1992) Interactions of polyomavirus middle T with the SH2 domains of the pp85 subunit of phosphatidylinositol-3-kinase, *J. Virol. 66*, 5485−5491.
21. Escobedo, J. A., Kaplan, D. R., Kavanaugh, W. M., Turck, C. W., and Williams, L. T. (1991) A phosphatidylinositol-3 kinase binds to platelet-derived growth factor receptors through a specific receptor sequence containing phosphotyrosine, *Mol. Cell. Biol. 111*, 125−132.
22. Kashishian, A., Kazlauskas, A., and Cooper, J. (1992) Phosphorylation sites in the PDGF receptor with different specificities for binding GAP and PI3 kinase *in vivo*, *EMBO J. 11*, 1373−1382.
23. Booker, G. W., Breeze, A. L., Downing, A. K., Panayotou, G., Gout, I., Waterfield, M. D., and Campbell, I. D. (1992) Structure of an SH2 domain of the p85α subunit of phosphatidylinositol-3-OH kinase, *Nature 358*, 684−687.
24. Hensmann, M., Booker, G. W., Panayotou, G., Boyd, J., Linacre, J., Waterfield, M., and Campbell, I. D. (1994) Phosphopeptide binding to the N-terminal SH2 domain of the p85α subunit of PI 3′-kinase: a heteronuclear NMR study, *Protein Sci. 3*, 1020−1030.
25. Nolte, R. T., Eck, M. J., Schlessinger, J., Shoelson, S. E., and Harrison, S. C. (1996) Crystal structure of the pi 3-kinase p85 amino-terminal SH2 domain and its phosphopeptide complexes, *Nat. Struct. Biol. 3*, 364−374.
26. Weber, T., Schaffhausen, B., Liu, Y., and Günther, U. (2000) NMR structure of the N-SH2 of the p85 subunit of phosphoinositide 3-kinase complexed to a doubly phosphorylated peptide reveals a second phosphotyrosine binding site, *Biochemistry 39*, 15860−15869.
27. Günther, U., Liu, Y., Sanford, D., Bachovchin, W., and Schaffhausen, B. (1996) NMR analysis of interactions of a Phosphatidylinositol 3′-kinase SH2 domain with phosphotyrosine peptides reveals interdependence of major binding sites, *Biochemistry 35*, 15570−15581.
28. Deleted in proof.
29. Yoakim, M., Hou, W., Songyang, Z., Liu, Y., Cantley, L., and Schaffhausen, B. (1994) Genetic analysis of a phosphatidylinositol 3-kinase SH2 domain reveals determinants of specificity, *Mol. Cell. Biol. 14*, 5929−5938.
30. Günther, U., Ludwig, C., and Rüterjans, H. (2000) NMRLAB: Advanced NMR data processing in Matlab, *J. Magn. Reson. 145*, 201−208.
31. Luz, Z., and Meiboom, S. (1963) Nuclear magnetic resonance study of the protolysis of triethylammonium ion in aqueous solution: order of the reaction with respect to solvent, *J. Chem. Phys. 39*, 366−370.
32. Carver, J., and Richards, R. (1972) General two-site solution for the chemical exchange produced dependence of T2 upon the Carr-Purcell pulse separation, *J. Magn. Reson. 6*, 89−105.
33. Jen, J. (1978) Chemical exchange and NMR T2 relaxation: the multisite case, *J. Magn. Reson. 30*, 111−128.
34. Davis, D., Perlman, M., and London, R. (1994) Direct measurements of the dissociation rate constant for inhibitor-enzyme complexes via the T1rho and T2 (CPMG) methods, *J. Magn. Reson., Ser. B 104*, 266−275.
35. Eck, M. J., Shoelson, S. E., and Harrison, S. C. (1993) Recognition of a high-affinity phosphotyrosyl peptide by the Src homology-2 domain of p56lck, *Nature 362*, 87−91.

BI0347499